Annals of Nuclear Energy 214 (2025) 111204

Contents lists available at ScienceDirect

Annals of Nuclear Energy

journal homepage: www.elsevier.com/locate/anucene

An overcooling transient analysis in a CAREM-like SMR core using Serpent/Subchanflow

Gianfranco Huaccho Zavala *, Victor Hugo Sánchez-Espinoza, Luigi Mercatali, Uwe Imke

Karlsruhe Institute of Technology, Institute of Neutron Physics and Reactor Technology, Hermann-von-Helmholtz-Platz 1, 76344 Eggenstein-Leopoldshafen, Germany

ARTICLE INFO

Keywords:
Monte Carlo
Multi-physics
Pin-by-pin
Serpent
Subchanflow
CAREM SMR
Coupled transient simulation

ABSTRACT

This work investigates a 50-s transient scenario in a CAREM-like SMR (Small Modular Reactor) core using a high-detail neutronic/thermal-hydraulic pin/subchannel model with the coupled tool Serpent/Subchanflow. The transient scenario is defined as a core overcooling, which can be described as a colder coolant front entering the reactor core and producing a rise in power due to the positive reactivity. The reactor core is initially at full power (100 MW), and the perturbations that originate the overcooling scenario are initiated by time-dependent boundary conditions of three variables: the coolant mass flow rate, the core inlet temperature, and the core outlet pressure. In the transient analysis with Serpent/Subchanflow, two different solutions with different time step lengths (0.05 s and 0.1 s) are investigated, and similar results are obtained. The reactor power increases by around 16%, the core average fuel temperature increases by 20 °C, and the core average coolant temperature decreases by 2.3 °C. The simulation has been performed in the Horeka supercomputer at KIT, using 760 cores, giving a maximum wall-clock simulation time of 19 days for the shorter time step length. As a final step, key parameters are compared at the beginning and end of the transient against two deterministic assembly-based solutions, namely PARCS/Subchanflow and PUMA/Subchanflow. The comparisons show that the three solutions are consistent one to each other since global parameters such as the power and the core average temperatures are in very good agreement. When comparing peak power values, one can also observe the advantage of the high-detail solution since this provides higher values for the fuel temperatures, void fraction, and lower DNB (Departure from Nucleate Boiling) ratio.

Contents

* Corresponding author.
E-mail address: gianfranco.zavala@kit.edu (G. Huaccho Zavala).

https://doi.org/10.1016/j.anucene.2025.111204
Received 26 August 2024; Received in revised form 13 November 2024; Accepted 11 January 2025
Available online 27 January 2025

1. Introduction

In the last decade, a lot of research and development was carried out within European projects to develop multi-physics coupling strategies to enhance the prediction accuracy of reactor physics simulations. These strategies consider very high detail of the geometry, i.e., at pin level, and with minor assumptions and simplifications. The multi-physics approach involves mainly the interaction between neutronics, thermal-hydraulics (TH), and fuel performance codes and revolves around the great versatility of Monte Carlo (MC) neutronic codes, in particular Serpent, and today's availability of High-Performance Computing (HPC) environments.

Previous European projects, such as the HPMC (High-Performance MC Methods for Core Analysis, started in 2011) (Demazière et al., 2020), the McSAFE (High-Performance MC Methods for SAFEty Analysis, started in 2017) (Sanchez-Espinoza et al., 2021b), and more recently, the McSAFER (High-Performance Advanced Methods and Experimental Investigations for the Safety Evaluation of Generic Small Modular Reactors, started in 2020) (Sanchez-Espinoza et al., 2021a) project, started chronologically with the proof-of-concept, development, optimization, and the verification and validation process of multi-physics coupling strategies for Light Water Reactor (LWR) applications, paving the way for the use on more industry-like and safety relevant applications (Sanchez-Espinoza et al., 2021a).

Part of the McSAFER project, where this work is confined, focuses on the numeric simulation side, employing multi-scale and multi-physics tools at different levels of detail, using conventional industry-like deterministic tools and the more recently high-detail approaches, to analyze the inherent safety features of SMRs under postulated design basis accident conditions. Four different Small Modular Reactor designs, namely the CAREM (CNEA), SMART (KAERI), F-SMR (CEA) and NuSCALE are selected for the project's purpose. This work focuses on a transient scenario analysis on a generic CAREM core.

CAREM (CAREM-25) is a project of the National Atomic Energy Commission (CNEA) of Argentina, that consists in the design, construction, and operation of an innovative, simple and small 100 MWth nuclear power plant (Giménez, 2014; IAEA, 2014). According to the actual status of SMRs development around the world (OECD-NEA, 2024), CAREM is part of a short list of SMR designs with higher level of progress and with an approved license for construction. CAREM's main design characteristic is the integrated self-pressurized primary cooling system, driven by natural circulation. Main primary system components such as the reactor core, the barrel, steam generators, and the control rod drive mechanism (CRDM) are inside the reactor pressure vessel (RPV) giving its integral characteristic. The defense in-depth concept has been internalized in the design since the conceptual engineering (Giménez, 2014), leading to safety systems that rely on passive features enhancing the safety significantly compared to actual nuclear power plants. Many intrinsic design characteristics contribute to the preclusion of classical initiating events, such as a large break loss of coolant accident (due to the absence of large orifices in the RPV), loss of flow (due to the natural circulation), rod ejection (innovative hydraulic in-vessel CRDM), and boron dilution accidents (absence of soluble boron in the coolant during normal operation) (Giménez, 2014).

The transient scenario consists of a reactivity insertion accident, it can be generally described as a cold water injection (core overcooling) during full power nominal operation conditions. Detailed description of the transient problem is presented in Section 3. The scenario is simulated using the embedded master–slave coupling tool Serpent/Subchanflow; a more detailed description of the multi-physics tool is presented in Section 4.

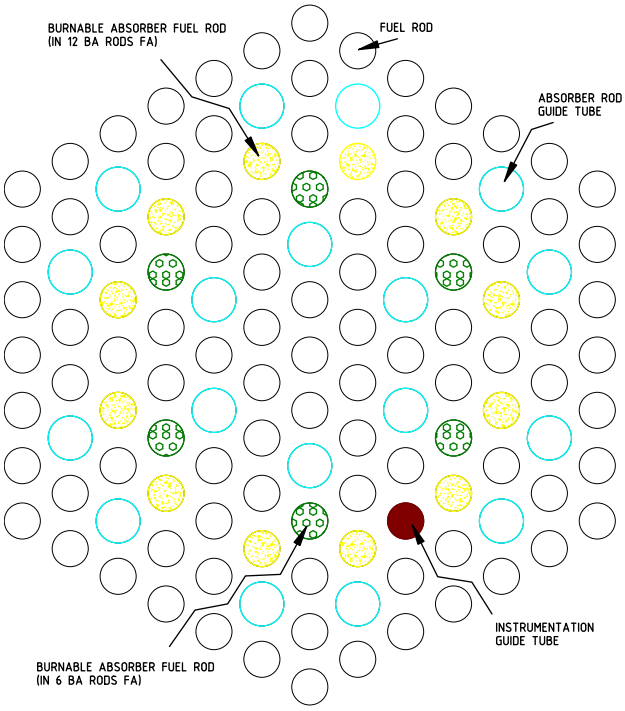

Fig. 1. Fuel assembly rod layout distribution.

The structure of this work is as follows: Section 2 presents a general description of the reactor core. Section 3 describes the transient problem. Section 4 describes the codes and their main characteristics and capabilities for simulating the coupled transient problem. Section 5 presents a detailed description of the developed models. Section 6 presents selected neutronic and thermal-hydraulic results and some comparisons against deterministic solutions. Finally, Section 7 presents a summary and main conclusions of the work.

2. Reactor core description

The CAREM-like core used in this study is briefly presented in this section. The core belongs to the beginning of cycle (BOC) with fresh fuel assemblies (FAs). The FAs are composed of UO_2 material with either 1.8% or 3.1% U_{235} enrichment. Burnable absorbers (BAs) are considered to minimize the initial BOC excess reactivity. The material selected for the BAs is a mixture of UO_2 (with natural enrichment) and Gd_2O_3. Only FAs with 3.1% enrichment have 6 or 12 BA-rods located strategically as shown in Fig. 1. Axially the BAs are concentrated in the central-lower part of the core, covering $1.1m$ of the $1.4m$ active height; remaining axial space is filled with regular fuel pellets. Additionally, each FA has 18 guide tubes, distributed in two rings, and one guide tube for instrumentation purposes, see Fig. 1.

The reactor core has a compact hexagonal layout distribution with 16 cm pitch distance between the FAs as show in Fig. 2. Four different FA types, differing mainly in the enrichment and in the amount of BAs, composed the reactor core, totaling 61 FAs. For reactivity control purposes, 25 control rod (CR) assemblies are distributed inside the core as shown in Fig. 3, resulting in 9 CR banks. There are two CR assembly

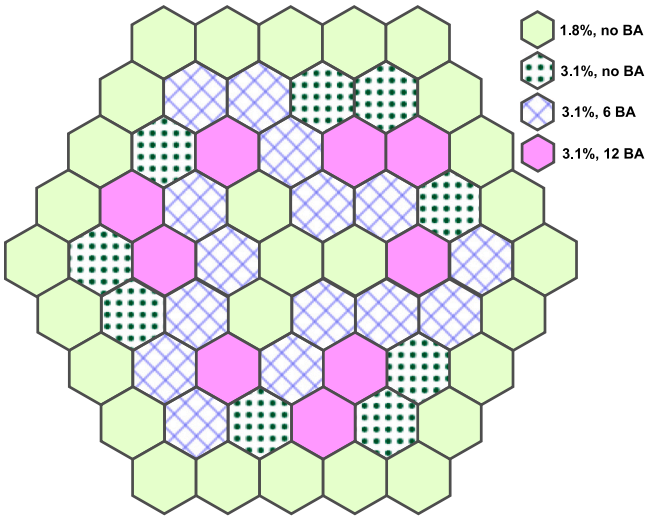

Fig. 2. Reactor core layout.

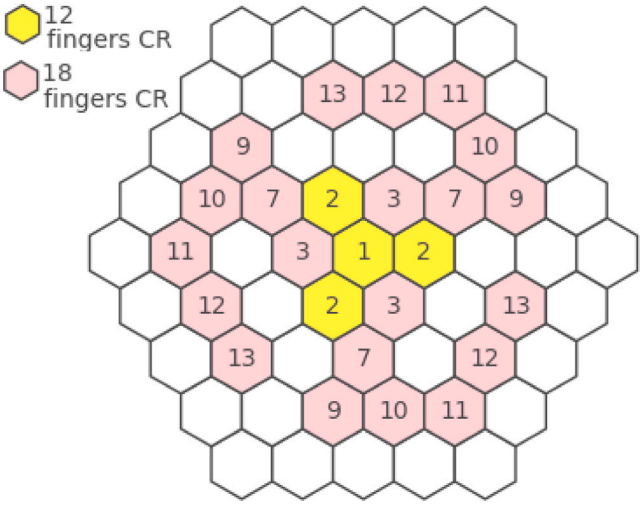

Fig. 3. Control rod banks layout.

types, they differ in the amount of absorber rods that could be either 12 or 18 (defined as fingers). In the CR assemblies with 12 absorber fingers only the external ring of guide tubes allocate absorber rods.

3. Description of the transient scenario

The transient scenario analyzed in this work can be described as a core overcooling during nominal full-power (HFP) operation. The initial HFP nominal condition is summarized in Table 1. The initiating event starts in the secondary side system, i.e., out of the RPV, generating in the primary coolant system, more specifically in the surroundings of the steam generators (allocated in the upper part of the RPV), a colder coolant front that will descend through the downcomer, and finally reaching the reactor core, as shown in Fig. 4. The colder coolant front will insert a positive reactivity to the system due to the coolant's lower temperature and higher density, producing a rise in power. The transient analysis is restricted to the reactor core domain, and the phenomena described are taken into account using time-dependent BCs for core outlet pressure, coolant mass flow rate, and coolant inlet temperature, see Figs. 5 and 6. Time-dependent BCs are specified for 50 s, and there are not other perturbations (as control rod movements) during the transient evolution.

Table 1
Reactor core HFP nominal condition.

Parameter	Value
Core thermal power	100 MW
Core outlet pressure	12.26 MPa
Core mass flow rate	423.6 kg/s
Core coolant inlet temperature	285.8 °C
Xenon concentration	Equilibrium
Control rod bank 1	50% extracted
Control rod bank 2	86% extracted
Control rod bank 9	68% extracted
Other control rod banks	Totally withdrawn

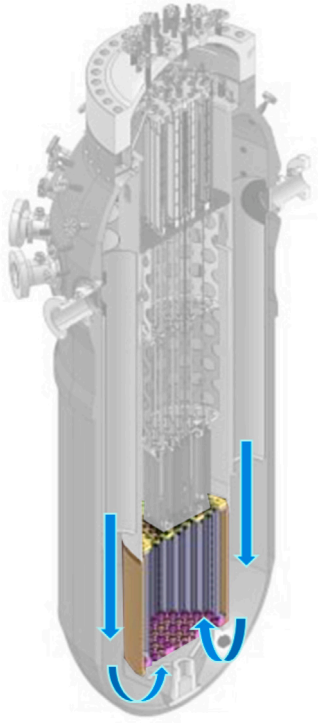

Fig. 4. RPV and internals. *Source:* Figure adapted from Magan et al. (2011).

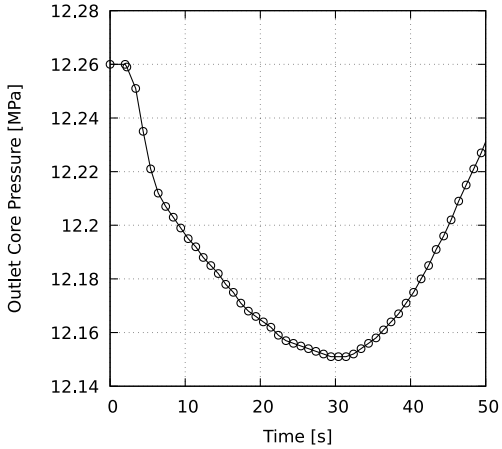

Fig. 5. Time-dependent core outlet pressure BC.

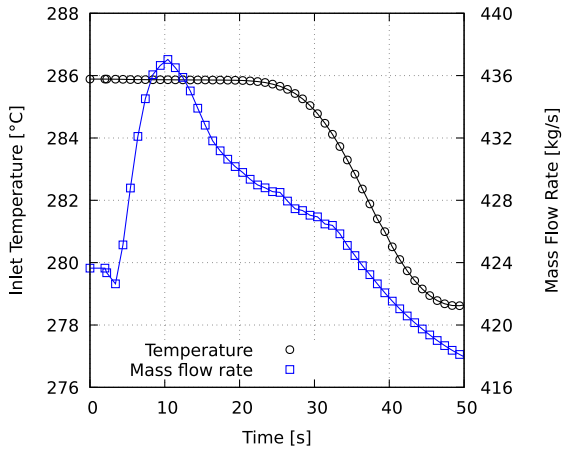

Fig. 6. Time-dependent inlet BCs for coolant.

4. Multiphysics tools

4.1. Serpent

Serpent is a multi-purpose, three-dimensional, continuous-energy Monte Carlo transport code developed since 2004 at VTT Technical Research Centre of Finland Ltd (Leppänen et al., 2015). It represents a state-of-the-art code aimed to perform static, burnup, and dynamic 3-D calculations using standard ACE format Nuclear Data Libraries (NDLs). Serpent was originally developed as a reactor physics code, but the scope has considerably broadened over the years, bringing the development of many advanced features (Serpent Wiki, 2024). The multi-physics (MP) capability and the time-dependent features are of interest for the purpose of this work. The basic idea of the Serpent's MP capability is to bring certain material properties into the Serpent model, e.g., material's density and temperature distribution, in order to have more realistic modeling during the simulation. The MP feature is wisely designed by an interface, which is defined on top of the Serpent's model, i.e., without altering the original model's geometry. Depending on how the external code solves the problem in terms of physics and geometry discretization, different interfaces are available in Serpent, i.e., point-wise, regular rectangular and hexagonal meshes, unstructured meshes, and many more. Examples of external codes coupled with Serpent via the MP interface are fluid dynamic (CFD) codes, channel thermal-hydraulic and system codes, and fuel performance codes (Leppänen et al., 2023; Leppänen, 2013b). The time-dependent (dynamic external source simulation mode) feature relies on an external source transport simulation with a user-specified time-binning structure to control the neutron population in noncritical systems, where this feature is usually exploited. The development was initially limited to prompt neutrons (Leppänen, 2013a), i.e., fast transient reactivity excursions, and then extended to account for delayed neutrons, tracking the precursor's source term (Valtavirta et al., 2016). Dynamic simulations in Serpent is performed in two steps: first, a criticality simulation is performed to generate the live neutrons and precursor sources needed for the second step, and then, the actual dynamic simulation is performed. This last feature, in combination with the MP interface, give the ground for coupled transient multi-physics simulations. The Serpent version 2.1.32 is used in this work.

4.2. Subchanflow

Subchanflow (SCF) is a subchannel three-equations and single-phase flow thermal-hydraulic code for steady-state and transient analysis developed at KIT, Germany (Imke and Sanchez, 2012). Subchanflow solves mass, momentum, and energy conservation equations along the axial discretization and between the neighbor lateral channels, i.e., cross-flow between channels. These equations together with a set of empirical correlations to calculate, for example, the pressure drop, heat transfer coefficients, void generation, etc., represent the system of equations of the single-phase (liquid/vapor mixture) flow model (Imke and Sanchez, 2012). The geometry is defined as a set of channels and rods with defined thermal-hydraulic parameters. A typical channel contains information such as its area, wetted and heated perimeter, and a list of its neighbor channels; a typical rod is defined by its material type, rod diameters, and a list of neighbored channels where the heat is released. The temperature profile inside each rod is calculated by dividing it into several radial rings and solving the heat equation in the radial direction by a finite volume method (Imke and Sanchez, 2012). An extension to fuel plates typically for the analysis of MTR (Material Testing Reactor) research reactors is also available in Subchanflow (Almachi et al., 2021). The Subchanflow version 3.7.1 is used in this work.

4.3. The Serpent/Subchanflow coupling

The Serpent/Subchanflow coupling was developed in the framework of the McSAFE project (Sanchez-Espinoza et al., 2021b) and main aspects of the implementation was first introduced in Ferraro et al. (2020a). The coupling relies in the capabilities and advanced features of both codes, e.g., the multi-physics interface in Serpent to interact with other codes and the Subchanflow aptness to be used as a library by other tool. The implementation consists in a high-level set of routines (coupling routines) developed in C language, where open door functions defined in the Serpent code, which allows to manage all main aspects of a coupled scheme, are managed by the coupling routines and Subchanflow is included and used as an external library, resulting in an embedded master–slave implementation (Ferraro et al., 2020a). The coupling tool has been widely tested under different benchmarks, e.g., steady-state analysis on a full VVER-1000 core (Ferraro et al., 2021a), reactivity insertion transient problems generated by a sudden control rod withdrawn on PWR and SMR cores (Ferraro et al., 2020b,c; Mercatali et al., 2023a), burnup analysis on PWR and VVER fuel assemblies (Ferraro et al., 2021b), and lastly on transient analysis on MTR fuel plate type (Almachi et al., 2024), showing the versatility of the tool.

For the purpose of this work, some details of a coupled transient simulation with Serpent/Subchanflow is presented. Fig. 7 shows the flow calculation for a coupled transient simulation with Serpent/Subchanflow. The Serpent's two step-approach for a dynamic simulation remains, and some extra considerations are taken into account during the process to consider the TH feedback. In the first step, successive iterations between Subchanflow and Serpent is performed, where the codes exchange respectively the Density-Temperature distribution (ρ, T)[1] and Power distribution (P) until the convergence is achieved. At this point, a power map file (*table_power_map.txt*, see Fig. 7) that contains the converged power distribution inside the core is saved. After the convergence is achieved, an extra iteration is performed to generate the neutron and precursor sources, i.e., Subchanflow reads the converged power map distribution and provides what it should be the converged (ρ, T) distribution into Serpent to generate the live and precursor neutron sources, additionally a new power map distribution can be obtained, which should be similar to the first one.

In the second step (transient) a fully-explicit iteration scheme is established for the transient simulation, Fig. 8 shows the time discretization structure for the two codes. It is important to clarify that Subchanflow predicts the TH parameters on time points $(t_0, t_1, \ldots, t_n)$, meanwhile Serpent runs a dynamic simulation in time bins $([t_0, t_1], [t_1, t_2], \ldots$

[1] For simplicity, (ρ, T) denotes the Temperature-Density distribution for the fuel and coolant.

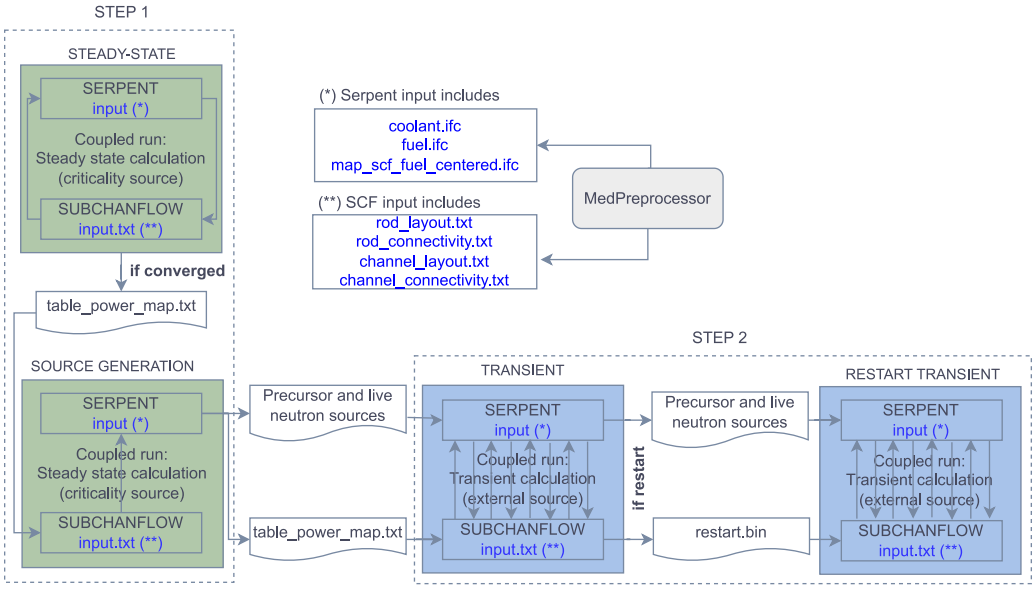

Fig. 7. Two-step approach for a transient simulation using Serpent/Subchanflow.

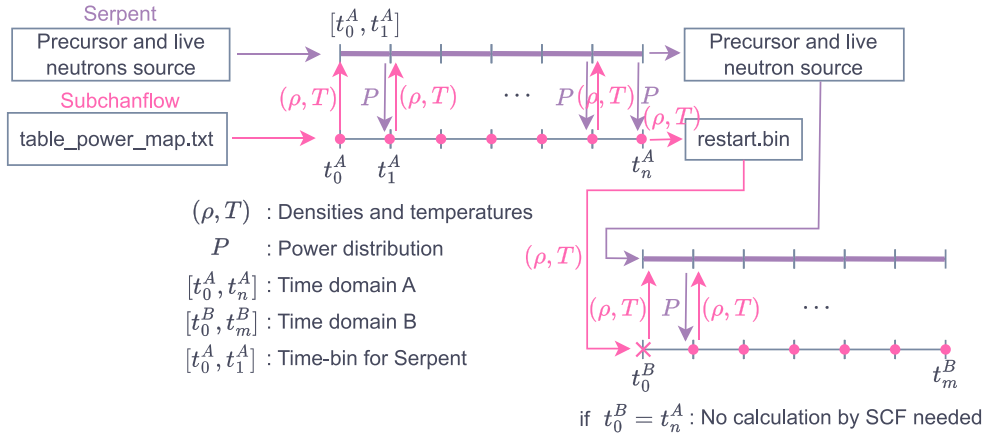

Fig. 8. Time domain discretization for a coupled transient simulation with Serpent/Subchanflow using the restart option. Considering that $t_0^B = t_n^A$, there is no need to predict again the TH parameters for t_0^B, transferring directly the (ρ, T)-fields back to Serpent.

$, [t_{n-1}, t_n]$). The coupled transient simulation starts as follows, Subchanflow starts reading the converged pin power distribution, as shown in Fig. 8, providing the initial (ρ, T) distribution at t_0 to Serpent. With this information, Serpent updates the material cross-sections according to the TH conditions and starts the dynamic simulation (external source mode) in the first time bin $[t_0, t_1]$. If needed, changes in the neutronic geometry, such as control rod movements can be considered during this time bin by Serpent, and only the TH parameters are kept constant until Serpent finishes the simulation in the time bin. In this time bin, a new pin power distribution is obtained and provided in return to Subchanflow, which predicts the new TH distribution for t_1, and the process continues until the transient simulation is completed.

Some transient simulations with Serpent/Subchanflow may require a restarting option to complete the simulation, specially when the total simulation time exceeds the maximum allowed wall-clock times usually encountered on multi-user high performance supercomputers (HPC). For the understanding of this restart capability, let us divide the total time domain in two parts, time domain *A* and *B* as shown in Fig. 8. At the end of the first time domain (t_n^A), all the TH state information is saved in a restart binary file (*restart.bin*, see Fig. 8), then the simulation can be restarted for the time domain *B*, reading directly all the TH information available in the binary file by Subchanflow and performing no calculation (in the first time point) and transferring the information directly to Serpent, as outlined in Fig. 8.

Setting up the inputs for a coupled simulation with Serpent/Subchanflow requires to take into considerations many files, e.g. interface files for the fuel and coolant, rod and subchannel layout, mapping files, time dependent boundary conditions, etc. As shown in Fig. 7, the Preprocessor program developed at KIT (Garcia et al., 2019) allows the generation of the files related to the geometry for both codes; these are the layout and connectivity files for rods and channels needed by Subchanflow, the MP interface files needed by Serpent, and the mapping file that links the two geometry domains defined by each code.

5. Developed models

5.1. Serpent model

Following the core description in Section 2, a 3D core model was developed in Serpent as shown in Figs. 9 and 10. The main assumptions and considerations taken into account are the following:

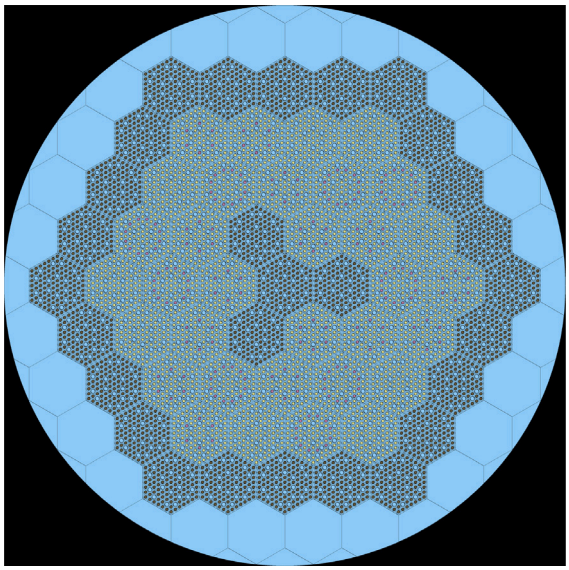

Fig. 9. XY plane from Serpent2 model in ARO condition.

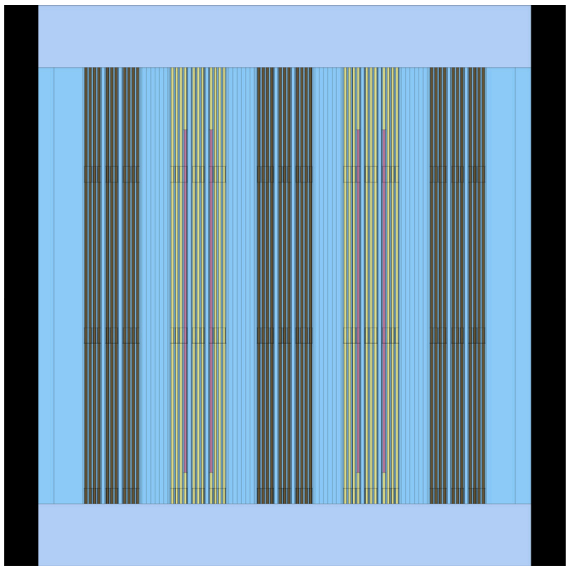

Fig. 10. XZ plane (rotated −30° in the Z-axis) from Serpent2 model. BAs covering the lower part of the active zone and grid spacers can be observed.

- The radial reflector is modeled as a cylinder with water properties. The barrel and downcomer are dismissed. Axial top and bottom reflectors are modeled as homogeneous material, composed of a mixture of water and Zircaloy.
- Three grid spacers are located at the active height and are modeled as an extra thickness in the cladding. A mixture between Inconel and Zircaloy is considered for the material composition. Grid spacers can be observed in Fig. 10.
- For Serpent criticality simulations (criticality source mode), 2000 cycles with 2×10^5 particles each are considered, with 200 inactive cycles for source convergence. For Serpent dynamic (transient) simulations (external source mode), 10^7 primary particles divided into 20 batches and distributed in 10 nodes or MPIs (Message Passing Interface) are considered.
- For the external TH feedback, multi-physic interfaces (IFC) are built to update TH properties in the fuel and the coolant materials, taking into account the fuel-centered TH model developed in Subchanflow. The IFC files are based on nested hexagonal meshes (IFC type 22 (Serpent Wiki, 2024)). The superimposed mesh for a single FA is built using a 15 × 15 hexagonal mesh, which is then nested on a bigger 9 × 9 hexagonal mesh to define the reactor core. Axially, the superimposed mesh is divided into 28 axial elements. The interface covers only the core's active zone.
- Equilibrium xenon concentration (Xe_{135}) at full power is considered. For simplicity, Xe_{135} is homogeneously distributed in the composition of the fissile materials.
- Detectors covering the active core are also defined to account for pin-power distribution.
- As far as the time binning for the population control during the transient simulation, two different solutions have been produced, corresponding to constant time bins of 0.05 s and 0.1 s over the 50 s transient.
- Control rod banks are in fixed position during the transient, as specified in Table 1.
- JEFF 3.1.1 ACE nuclear data library was considered.

5.2. Subchanflow model

Fig. 11 shows the fuel-centered model developed in Subchanflow using its Preprocessor. Higher detail of the subchannel and a 3D view representation are shown in Figs. 12 and 13. The following assumptions and considerations are taken into account:

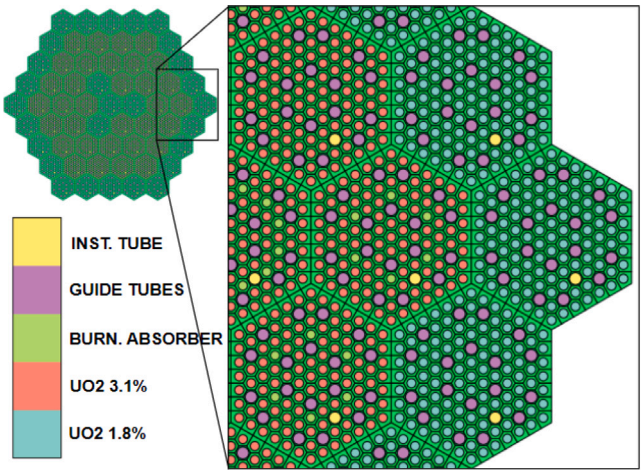

Fig. 11. Subchanflow fuel-centered model at pin/subchannel level.

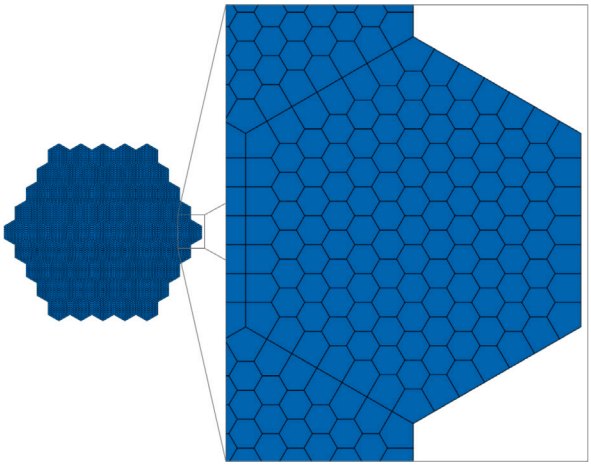

Fig. 12. Subchanflow subchannel layout in the fuel-centered model.

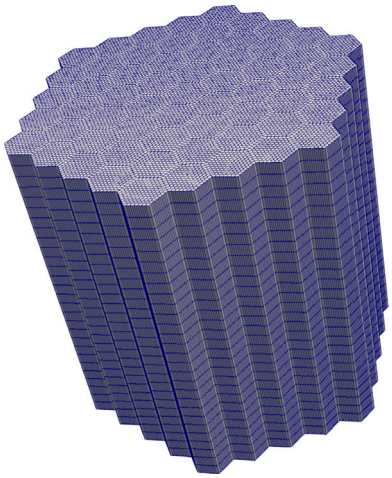

Fig. 13. Subchanflow subchannel 3D-view with axial discretization details.

- In the fuel-centered TH model, every pin-rod is surrounded by water and defines a rod/subchannel element. A total amount of 7747 (61 FA × 127 rods) and 7747 subchannels are considered in the TH model, both rods and subchannels are divided into 28 axial elements (5 cm per element).
- For the heat conduction inside the fuel rod, 10 radial nodes are considered in the fuel pellet, and 2 nodes for the cladding. Default UO_2 and Zircaloy materials available in Subchanflow with temperature-dependent properties (e.g., conductivity, specific heat, thermal expansion, emissivity) are selected for the fuel and the cladding. Subchanflow performs a simple gap conductance model and simple thermo-mechanics to predict the fuel-cladding gap width. For rods without fuel (e.g., instrumentation and control rod guide tubes) internal constant water properties are considered.
- Since Subchanflow calculates a radial temperature profile inside the fuel pellet and one single temperature value per fuel rod is needed in Serpent for the TH feedback (on-the-fly temperature treatment (Viitanen and Leppänen, 2014)). An effective Doppler temperature, defined as $T_{doppler} = 0.7{\times}T_s{+}0.3{\times}T_c$, is considered for the cross sections adjustments, where T_s, and T_c are the surface and centerline fuel temperature for each fuel pellet, respectively.
- Some of the main correlations selected in Subchanflow for the simulation are, *Blasius* for the turbulent friction, *Dittus Boelter* for the heat transfer, and *Westinghouse-3* correlation for the critical heat flux. For the coolant water properties, the *IAPWS-97* standard is selected.
- The time-dependent boundary conditions (BCs), i.e., inlet coolant temperature, mass flow rate, and outlet core pressure, are specified in text files in a simple column format. Interpolation between the two nearest points is considered, when the BCs are not defined at a specific time.

5.3. Extra coupling considerations

For the steady-state simulations, a convergence criteria considering the difference (in some selected parameters) between the last two iterations are considered. The parameters selected to account for the convergence are the core reactivity, the Doppler fuel temperature, the coolant temperature, and the coolant density. An L_2-norm is considered for the TH parameters (Ferraro et al., 2020a). The selected convergence criteria is:

- $\Delta\rho < 10$ pcm
- $\Delta T^{doppler} < 5$ °C in L_2 norm.

Table 2
Names, abbreviations, and definitions of main parameters derived from the TH model.

Parameter (Abreviation)	Definition
Fuel rod index	$i : \{1, 2, \ldots, I\}; I = 6786$
Channel index	$j : \{1, 2, \ldots, J\}; J = 7747$
Axial cell index	$k : \{1, 2, \ldots, K\}; K = 28$
Centerline fuel Temperature (Tfuelc)	T_{ik}^{fuelc}
Outer surface fuel Temp. (Tfuelo)	T_{ik}^{fuelo}
Internal surface cladding Temp. (Tcladi)	T_{ik}^{cladi}
Outer surface cladding Temp. (Tclado)	T_{ik}^{clado}
Coolant Temperature (Tcool)	T_{jk}^{cool}
Void fraction (voidf)	f_{jk}
DNB ratio (DNBr)	DNB_{ik}
Doppler Temperature (Tdop)	$T_{ik}^{dop} = 0.3T_{ik}^{fuelc} + 0.7T_{ik}^{fuelo}$
Cladding Temperature (Tclad)	$T_{ik}^{clad} = 0.5T_{ik}^{cladi} + 0.5T_{ik}^{clado}$
Max. Tfuelc	$max\{T_{ik}^{fuelc}\}$
Max. Tdop	$max\{T_{ik}^{dop}\}$
Ave. Tdop	$\frac{1}{I\times K}\sum_{i,k} T_{ik}^{dop}$
Max. Tcladi	$max\{T_{ik}^{cladi}\}$
Max. Tclad	$max\{T_{ik}^{clad}\}$
Ave. Tclad	$\frac{1}{I\times K}\sum_{i,k} T_{ik}^{clad}$
Max. Tcool	$max\{T_{jk}^{cool}\}$
Ave. Tcool	$\frac{\sum_{j,k} V_{jk}\times T_{jk}^{cool}}{\sum_{j,k} V_{jk}}$, V_{jk} : *jk-channel volume*
Max. voidf	$max\{f_{jk}\}$
Ave. voidf	$\frac{\sum_{j,k} V_{jk}\times f_{jk}}{\sum_{j,k} V_{jk}}$
Min. DNBr	$min\{DNB_{ik}\}$

- $\Delta T^{coolant} < 2$ °C in L_2 norm.
- $\Delta\rho_{coolant} < 0.01$ g/cm^3 in L_2 norm.

Additionally, for the steady-state simulations, a relaxation factor of 0.5 was used to accelerate the convergence in the TH parameters. For the transient simulation, no relaxation factor is considered.

5.4. Hardware environment

The simulations have been performed in the Horeka supercomputer at KIT, where each CPU is an Intel Xeon Platinum 8368 with 76 cores per node. All nodes are interconnected through the InfiniBand 4X HDR 200 GBit/s (Horeka, 2024). All the simulations were performed with 76 OMP and from 1 to 10 nodes, depending on the case.

6. Results and discussion

This section presents the results starting with a pure neutronic criticality characterization using Serpent stand-alone, then the TH feedback is added to characterize the steady-state at full power condition, which is also the transient's initial condition, and finally, the transient results are presented. Since a high-detail model is considered for the core analysis, some definitions and how maximum and average values of main TH parameters are calculated are summarized in Table 2. The same problem has been performed and analyzed with deterministic tools, namely PUMA/Subchanflow and PARCS/Subchanflow, as part of the first stages of the McSAFER project, and the main results have been presented in Fridman et al. (2024), Mercatali et al. (2023b). The primary motivation of this work is to present in detail the Serpent/Subchanflow solution for this transient problem, which is the main focus of the results section. Nevertheless, as a final step, the main TH parameters are compared at the beginning and end of the transient (BOT, EOT) between the deterministic assembly-level and Monte Carlo pin-level solutions coupled all together with Subchanflow.

6.1. Serpent stand-alone HFP characterization

For the pure neutronic criticality characterization, generally the assumptions and considerations specified in Section 5.1 are considered;

Table 3
Serpent stand-alone reactivity results.

Control rod configuration	Reactivity $\pm$ 1σ [pcm]
Completely withdraw (ARO)	5861 ± 3
Bank 1: 50%, Bank 2: 86%, and Bank 9: 68%	692 ± 4
Completely inserted (ARI)	-19977 ± 5

Table 4
Serpent/Subchanflow steady-state converged results for the partially inserted control rod banks.

Parameter	Serpent/SCF
Core reactivity [pcm]	169 ± 4
Ave. Tdop [°C]	473.3
Ave. Tclad [°C]	336.9
Ave. Tcool [°C]	310.7
Ave. coolant density [g/cm^3]	0.6747

additionally constant TH properties, i.e., temperatures and densities, must be defined. Nominal conditions were defined in Fridman et al. (2024), considering 921 K for the fuel temperature and (578.15 K, 0.702 g/cm^3) for the coolant temperature and density. The core criticality is evaluated considering three different control rod (CR) configurations, i.e., CRs completely withdrawn (ARO), CRs completely inserted (ARI), and some CR banks partially inserted. The criticality results for the three cases are presented in Table 3.

The ARO condition gives the core excess reactivity in the HFP condition with equilibrium xenon; BAs help to minimize the initial excess reactivity, reducing the number of CRs needed to compensate for the 5800 pcm excess reactivity. This excess reactivity should compensate for the U_{235} consumption during the CAREM's 14-month cycle length (IAEA, 2014). The ARI condition gives a reasonable margin of negative reactivity, giving a CR banks' worth of around 25800 pcm. For the CR banks partially inserted (CR banks positions for the transient), a supercritical condition of 690 pcm is obtained. The values presented in this subsection represent a starting point solution for the following results, where the TH feedback will be included.

6.2. Serpent/Subchanflow steady-state HFP characterization

Taking into account the considerations given in Section 5.2 for the THs, a steady-state simulation is performed using Serpent/Subchanflow. Only the case with some partially inserted CR banks is considered, with the objective of characterizing the core's initial state previous to the transient scenario. The steady-state converged solution is achieved after seven iterations for the specified convergence criteria, and core criticality and average TH parameters are presented in Table 4.

Comparing the results against the Serpent stand-alone, Subchanflow predicts a 174 °C lower core average fuel temperature and a 6 °C higher coolant temperature, resulting in a lower coolant density that reduces (on average) the moderation effect. The differences mentioned in the THs result in a 523 pcm lower core reactivity, obtaining a slightly supercritical condition (+169 pcm) for the transient's initial state.[2]

Converged radial pin-power distribution is shown in Fig. 14, where the presence of partially inserted control rods and BAs (6 or 12 UO_2-GdO_3 pins) are clearly observed. Higher power is obtained in FAs with higher enrichment (3.1%) and without BAs, and as expected, lower power is obtained in FAs with lower enrichment (1.8%) or zones with the presence of CRs or BAs. Fig. 15 shows the axially average relative uncertainty (1σ statistical deviation) in the pin power distribution, where zones with higher statistical uncertainty are obtained in low power regions, i.e., lower statistics.

[2] For the transient simulation, which should start from a critical condition, initial slightly supercritical condition is handled scaling the fission neutron production. The *set keff* command was used in Serpent

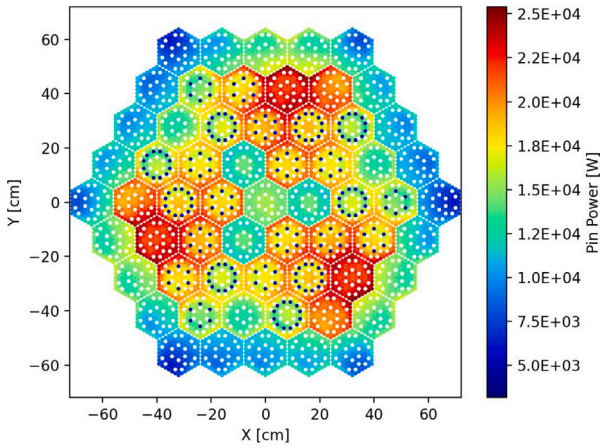

Fig. 14. Steady-state axially integrated pin-power distribution.

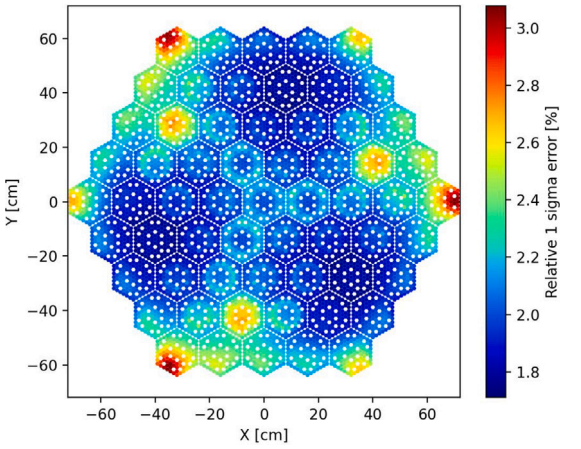

Fig. 15. Axially averaged relative statistical uncertainty distribution map.

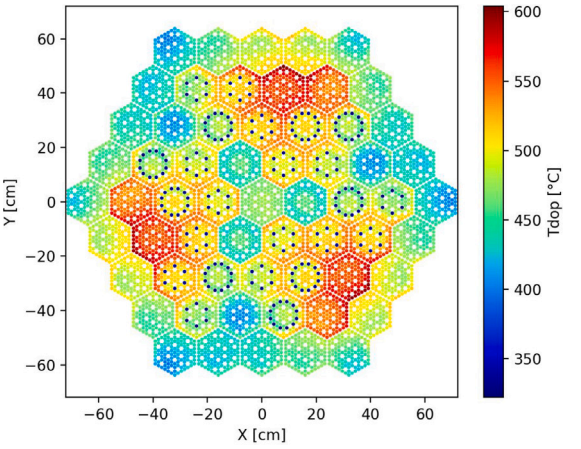

Fig. 16. Doppler temperature distribution map in the 14th axial cell.

Fig. 16 shows the Doppler temperature distribution in the 14th axial cell (the core's axial middle cell), reflecting the same distribution as the pin power since higher fuel temperatures are expected in fuel pins with higher power. Additionally, Fig. 17 shows the fuel-cladding gap distribution predicted by Subchanflow, where shorter gap widths are predicted in the hotter fuel rods.

An interesting design characteristic in CAREM is the generation of some vapor in the core, achieving saturated conditions at the core

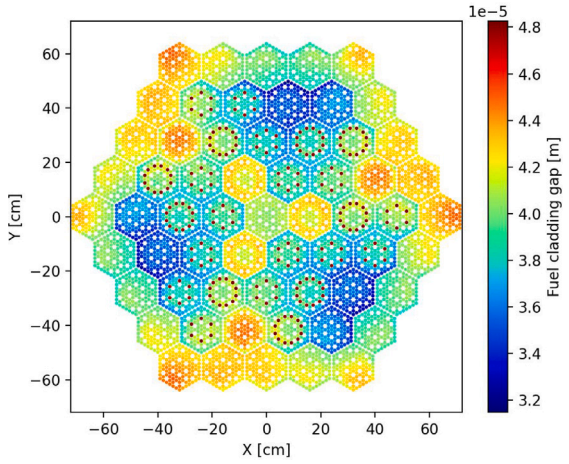

Fig. 17. Fuel-cladding gap width distribution map in the 14th axial cell.

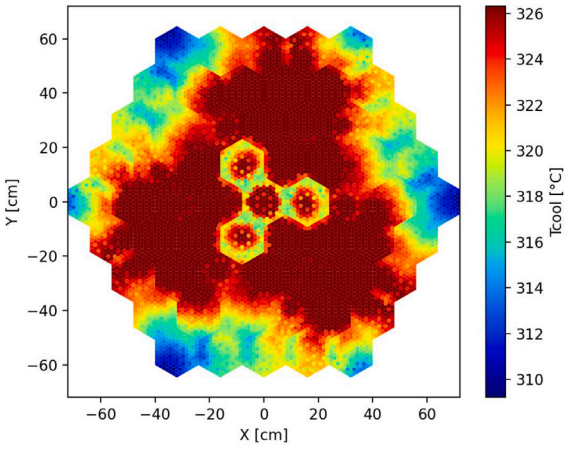

Fig. 18. Coolant temperature distribution map in the 28th axial cell.

outlet. Then, the vapor generation is increased in the chimney due to the flashing phenomenon, enhancing the natural circulation in the primary circuit (Marcel et al., 2013). Figs. 18 and 19 show the coolant temperature distribution and the thermodynamic quality (x)[3] in the last axial cell of the core ($k = 28$); it is interesting to observe that a large part of the coolant leaving the core is saturated ($x = 0$) coexisting with some super-heated vapor ($x > 1$). Figs. 20 and 21 show the vapor mass quality and the void fraction in the last axial cell of the core ($k = 28$).

6.3. Serpent/Subchanflow overcooling transient

Due to the expensive Monte Carlo calculations, particularly for this relatively long transient problem, special attention was paid to the time binning for the population control in Serpent. Previous results of this transient problem using standard deterministic tools (Fridman et al., 2024; Mercatali et al., 2023b), predict an increase in power of less than 20% in the 50 s period, and relatively no significant changes or fast gradients in the TH parameters were observed. Therefore, the neutron population could be handled in relatively longer time bins, and no need for a fast update of the THs into the neutronics is expected. Two cases (cases A and B) with different time bin sizes are analyzed to

[3] Thermodynamic quality is defined as $x = \frac{h-h_f}{h_g-h_f}$, where h is the mixture specific enthalpy. The subscripts f and g refer to saturated liquid and saturated vapor respectively.

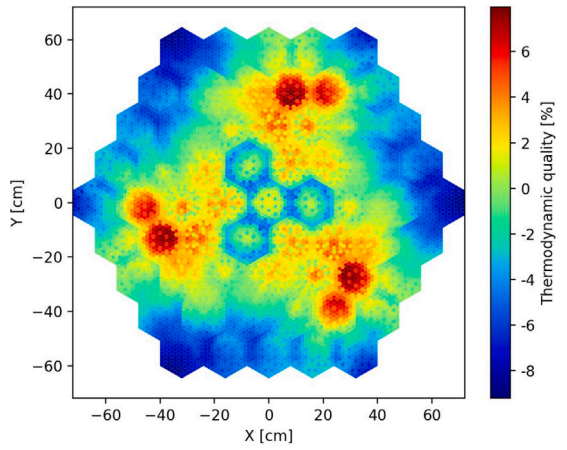

Fig. 19. Thermodynamic quality distribution map in the 28th axial cell.

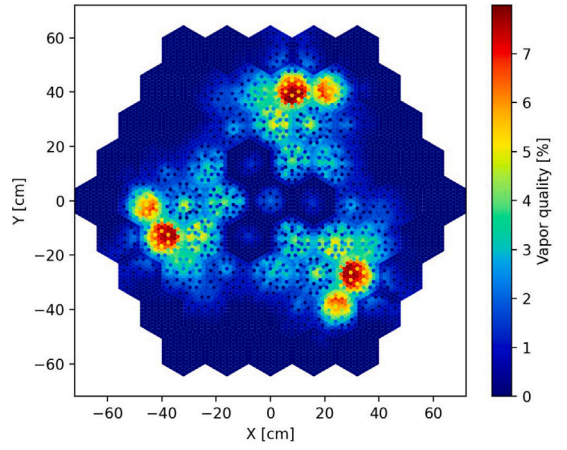

Fig. 20. Mass vapor quality distribution map in the 28th axial cell.

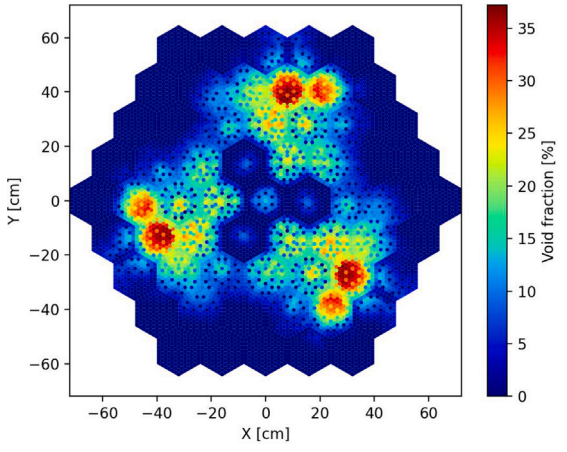

Fig. 21. Void fraction distribution map in the 28th axial cell.

evaluate the minimum and reasonable time interval that should be used for this particular problem. Constant time bins of 0.05 s and 0.1 s are considered, and for simplification, the same bins' lengths are considered as the time steps in Subchanflow. Regarding statistics for the transient simulation (external source mode), 10^7 primary particles divided into 20 batches and distributed in 10 nodes or MPIs are considered. The complete 50 s time domain was subdivided into smaller time interval domains such that the HPC cluster's maximum wall-clock simulation

Table 5
Details of the selected parameters for cases A and B.

Parameter	Case A	Case B
Total simulation time [s]	50	50
Time intervals [#]	1000	500
Time bin length [s]	0.05	0.1
Primary particles [#]	10^7	10^7
Number of batches [#]	20	20
Number of MPIs [#]	10	10
Number of OMPs [#]	76	76
Total cores [#]	760	760
Time domain subdivision [s]	$[0, 5]$, $< 5\ m, 5(m+1)]$	$[0, 5]$, $< 5n, 5(n+2)]$, $< 45, 50]$
	$m = \{1, 2, \ldots, 9\}$	$n = \{1, 3, 5, 7\}$
Restart calculations [#]	9	5

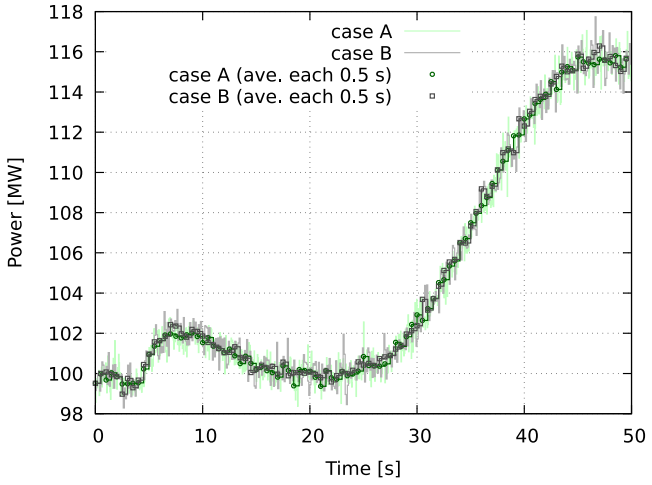

Fig. 22. Total power evolution in time. Average values every 0.5 s are also plotted for a more clearly visualization since the power evolution presents some noisy behavior.

time was not exceeded. Intervals of 5 s for case A and 10s for case B were considered. The main set-up parameters for the two cases is presented in Table 5.

Both simulations were launched using the same amount of CPU resources in a supercomputer environment specified in Section 5.4, giving wall-clock simulation times of 19 and 10 days for cases A and B, respectively.

Fig. 22 shows the total core power evolution; both solutions are practically equivalent. An initial increase in power is observed at around 5 s in coincidence with the increasing in the core's mass flow rate. A second, more significant rise in power is observed in the last 20 s of the transient due to the coolant's colder temperature front entering into the core. The average relative uncertainty (1σ statistical deviation) for the total core power is less than 0.6% during the transient scenario, and pin power statistical uncertainties increase up to a maximum value of 4% with an average value of 2%, as shown in Fig. 23. Slightly smaller uncertainties are observed for case B since better statistics are expected on larger time bins.

It was of interest for the authors to quantify the perturbation in the system in terms of reactivity. According to the Serpent's discussion forum, the k_{eff} estimators usually encountered in the Serpent's output (e.g., IMP_KEFF) represent the eigenvalue solution of the transport equation, which is not solved during a dynamic simulation (Serpent Forum, 2024). The forum also suggests an alternative way to calculate the time-dependent k_{eff}, defining Serpent detectors to account for neutron production (e.g., fission neutron production) and losses (e.g., capture reactions, leakage) in every time bin. Unfortunately, detectors were not set up for cases A and B, and due to the expensive solution in terms of CPU resources to run it again, an alternative method to

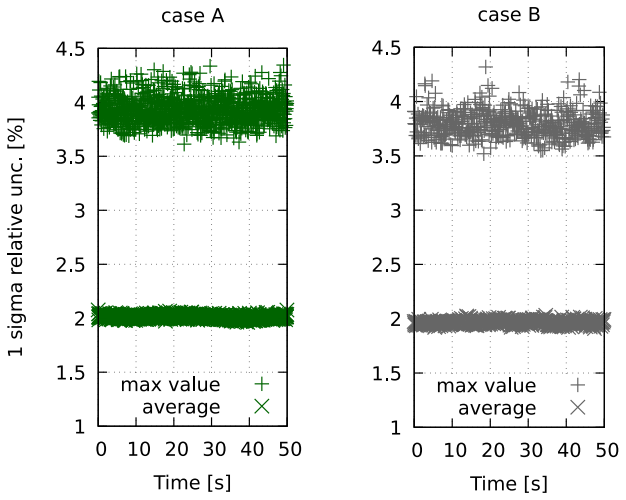

Fig. 23. Maximum and average pin power relative statistical uncertainty.

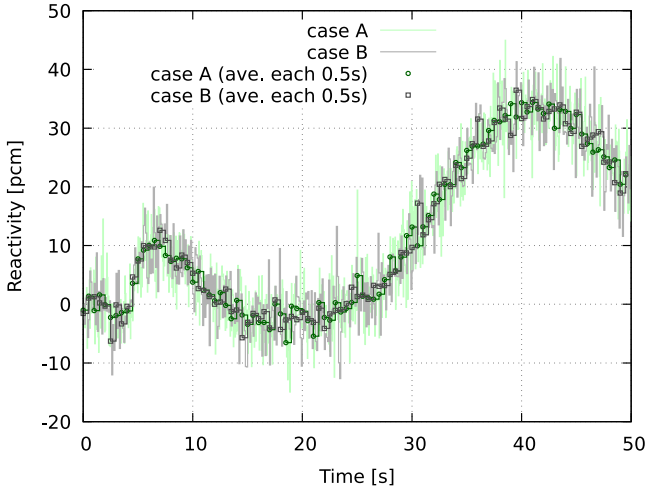

Fig. 24. Core reactivity evolution in time derived from the power evolution using the inverse kinetic method.

compute the reactivity evolution is presented. The alternative solution is based on the inverse kinetic method derived from the point kinetic equations (Stacey, 2006); this approach is typically applied in experimental facilities for reactivity measurements, where the signal from a neutron detector together with a set of kinetic constants that characterize the core are used to deduce the reactivity. In our case, the core power evolution presented in Fig. 22 and the 8-group kinetic constants generated during the steady-state step are the input parameters to deduce the reactivity evolution. The kinetic parameters are shown in the Appendix. The reactivity evolution is shown in Fig. 24. Again, the perturbations in the reactivity caused initially by an increase in the mass flow rate and then by the dropping in the coolant inlet temperature are clearly observed. It can be concluded that changes in the TH boundary conditions cause perturbations in the system of less than 40 pcm.

The second part of the results show the TH parameters derived from Subchanflow outputs for cases A and B. In general, no appreciable differences are observed between these two cases during the transient evolution. Core average and maximum values at pin/subchannel level, according to the definitions presented in Table 2, are presented:

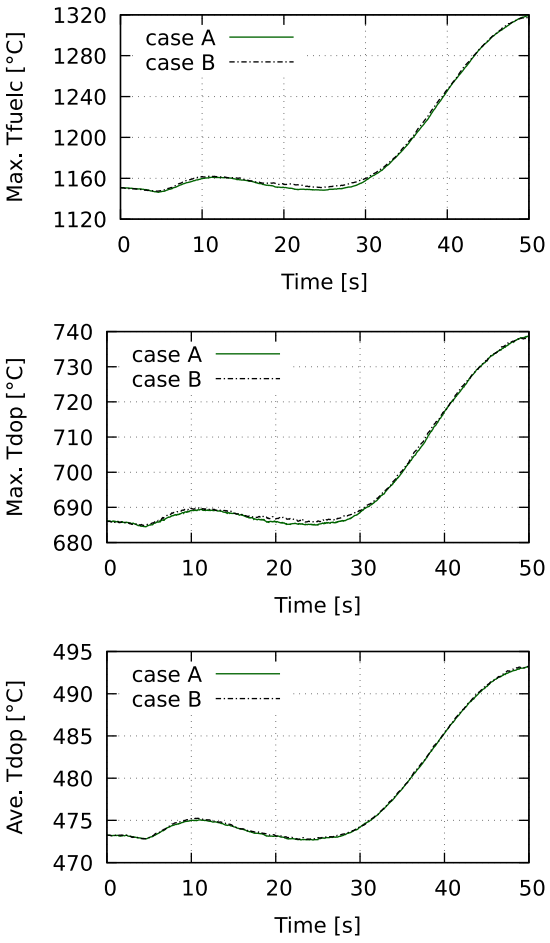

Fig. 25. Maximum and core average fuel temperature evolution in time.

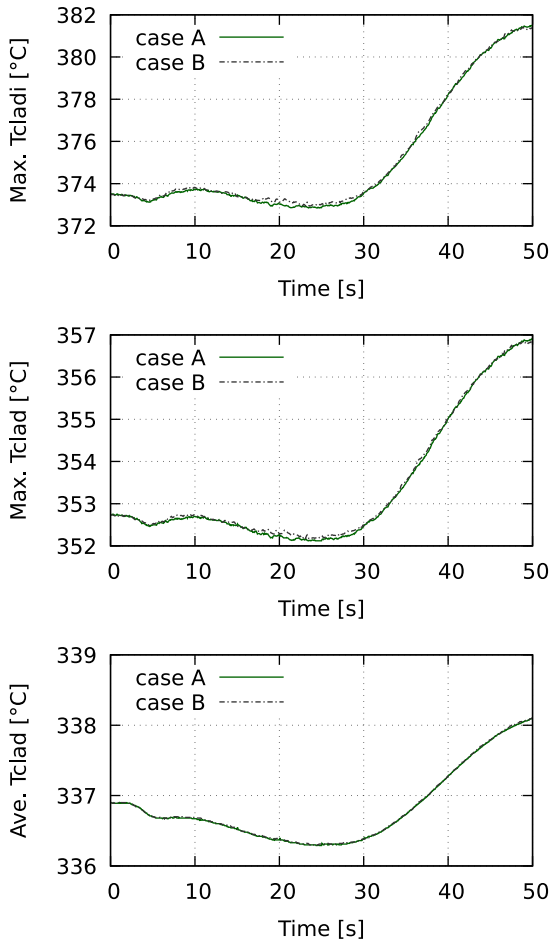

Fig. 26. Maximum and core average cladding temperature evolution in time.

- Fig. 25 shows different plots related to the fuel temperature, these are: the maximum centerline temperature (*Max. Tfuelc*), the maximum Doppler temperature (*Max. Tdop*), and the core average Doppler temperature (*Ave. Tdop*). The first one indicates the hottest temperature achieved in the fuel, which is located in the centerline of a fuel pellet. The maximum temperature at the beginning and end of transient (BOT, EOT) are respectively 1151 °C and 1319 °C, having an increase of 168 °C. The increase in *Max. Tdop* and *Ave. Tdop* are approximately 52 °C and 20 °C, respectively.
- Fig. 26 shows different plots related to the cladding temperature, these are the maximum internal cladding temperature (*Max. Tcladi*), the maximum cladding temperature (*Max. Tclad*), and the core average cladding temperature (*Ave. Tclad*). The first one indicates the hottest temperature achieved for the cladding in the core, i.e., internal side of the cladding. The maximum temperature achieved at BOT and EOT are 373 °C and 381 °C, respectively.
- Fig. 27 shows the evolution of the maximum coolant temperature (*Max. Tcool*) and the core average (*Ave. Tcool*). In the steady-state core characterization, it was observed that some part of the coolant in the 28th axial cell (core outlet) is in saturated conditions, as is also the case during the transient evolution. In the saturated conditions, the coolant temperature depends only on the pressure, as seen in the figure where the *Max. Tcool* has a similar shape evolution as the core outlet's pressure boundary condition. The *Ave. Tcool* at BOT and EOT are 310.7 °C and 308.4 °C, respectively.
- Fig. 28 shows the maximum and core average void fraction (*Max. voidf*, *Ave. voidf*). A significant difference between the maximum and the average value is observed. The *Max. voidf* at the BOT and EOT are 37.2% and 39.3%, respectively, and for the *Ave. voidf*, 2.9% and 3.3%.

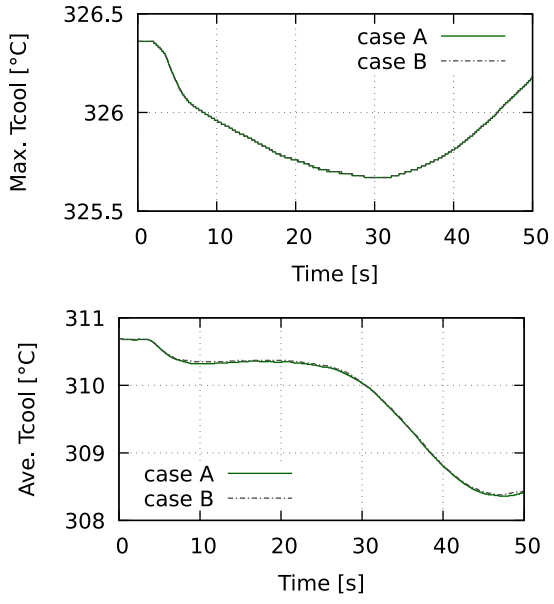

Fig. 27. Maximum and core average coolant temperature evolution in time.

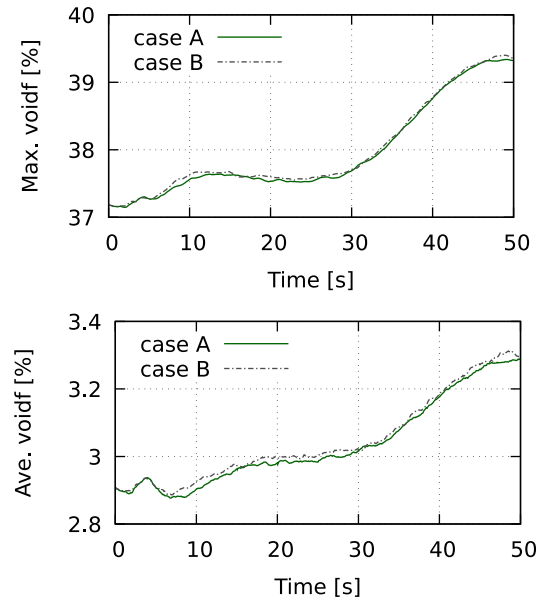

Fig. 28. Maximum and core average void fraction evolution in time.

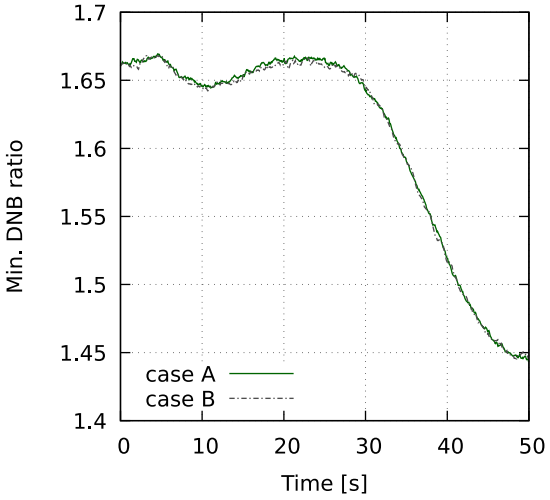

Fig. 29. Minimum DNB ratio evolution in time.

- Fig. 29 shows the evolution of the minimum DNB ratio, i.e., the fuel rod cell with the highest heat flux and closer to the critical heat flux. The minimum DNB at BOT and EOT are 1.66 and 1.44, respectively; representing a decrease of 13%.

Finally, selected results at BOT and EOT are compared against the deterministic PARCS/Subchanflow and PUMA/Subchanflow solutions. PARCS and PUMA are 3D core simulators that solve a reactor core by diffusion approximation following the classic two-step approach, where homogenized and condensed cross-sections are generated in the first step using cell codes. Both PARCS and PUMA have been coupled with Subchanflow for the TH feedback, where each FA is simulated as a single TH channel with a representative fuel rod for the thermal behavior, resulting in 61 channels and 61 representative fuel rods for the core model. References (Fridman et al., 2024; Mercatali et al., 2023b) further detail the models and methodologies followed in the deterministic solutions.

A comparison of the results at BOT and EOT are summarized in Tables 6 and 7, respectively, where relative differences respect to the Serpent/Subchanflow (case A) solution are considered. In general, global parameters such as the core power or core average temperatures are in very good agreement between the solutions, demonstrating the good consistency of the three solutions.

Table 6
Comparison results at the BOT. *pp* means percent point.

Parameter	Beginning of transient ($t = 0$ s)		
	Serpent/SCF	PARCS/SCF	PUMA/SCF
Power	(98.6 ± 0.6) MW	+1.4%	+1.4%
Max. Tfuelc	1150.9 °C	–	–
Max. Tdop	686.2 °C	−5.0%	−5.1%
Ave. Tdop	473.3 °C	+0.2%	+0.4%
Max. Tcladi	373.53 °C	–	–
Max. Tclad	352.75 °C	−0.8%	−0.7%
Ave. Tclad	336.9 °C	+0.1%	+0.1%
Max. Tcool	326.36 °C	0.0%	0.0%
Ave. Tcool	310.69 °C	+0.1%	+0.2%
Max. voidf	37.18%	−29.4*pp*	−34.0*pp*
Ave. voidf	2.9085%	+5.0*pp*	+11.9*pp*
Min. DNB	1.6605	+18.9%	+10.3%

Table 7
Comparison results at the EOT.

Parameter	End of transient ($t = 50$ s)		
	Serpent/SCF	PARCS/SCF	PUMA/SCF
Power	(114.5 ± 0.7) MW	+0.6%	+0.7%
Max. Tfuelc	1319.4 °C	–	–
Max. Tdop	738.69 °C	−4.8%	−6.2%
Ave. Tdop	493.18 °C	+0.2%	−0.5%
Max. Tcladi	381.49 °C	–	–
Max. Tclad	356.9 °C	−1.0%	−0.9%
Ave. Tclad	338.1 °C	+0.1%	+0.1%
Max. Tcool	326.18 °C	0.0%	0.0%
Ave. Tcool	308.42 °C	+0.2%	+0.2%
Max. voidf	39.326%	−29.0*pp*	−33.1*pp*
Ave. voidf	3.2879%	+5.5*pp*	+13.0*pp*
Min. DNB	1.4436	+20.2%	+12.7%

When moving to peak-value comparisons, some discrepancies are expected due to the different element volume sizes of the modeling, i.e., pin-level and FA-level. These differences can be summarized as follows:

- PARCS/Subchanflow and PUMA/Subchanflow predict around 5% lower temperature in *Max. Tdop*.
- PARCS/Subchanflow and PUMA/Subchanflow predict around 1% lower temperature in *Max. Tclad*.
- For all the solutions the computed *Max. Tcool* is identical since all the tools predict saturated water conditions.
- PARCS/Subchanflow and PUMA/Subchanflow predict around 30*pp* (percent points) lower *Max. voidf*.
- Serpent/Subchanflow predicts the lowest DNB ratio. However, some discrepancies are observed. PARCS/Subchanflow predicts a value around 20% bigger, whereas PUMA/Subchanflow only predicts an 11% bigger value, which may suggest that different peak factors (or no factors) could have been considered in the deterministic solutions.

7. Summary and conclusions

A neutronic/TH characterization for an SMR 100$MWth$ CAREM-like reactor core has been performed using high-detail (pin/subchannel) models with the coupled tool Serpent/Subchanflow. The core characterization started with a steady-state analysis at HFP condition, followed by the 50-s overcooling transient. According to the literature and to the best knowledge of the authors, the scenario analyzed in this

work represents the longest transient that has up to now ever been simulated with a high-detail pin-by-pin neutronic and subchannel-by-subchannel TH coupled code. It is important to remark that in the 50-s transient evolution, the reactor core state remains close to the HFP nominal condition, increasing the power by less than +16%, the *Ave. Tdop* by +20 °C, and the *Ave. Tcool* by −2.3 °C. These particular characteristics give us an idea of the relatively slow dynamic of the transient. Therefore, a thinner resolution in time than 0.05 s (case A) is not necessary for the analysis of this type of scenario, as it is the case in scenarios with high reactivity insertion, like control rod ejection transients, where the power increases exponentially, bringing fast and higher changes in the THs, requiring higher resolution in time for better capturing the transient's phenomenology. It is also known that, as the time bin gets shorter in a dynamic Monte Carlo simulations, the statistical uncertainty increases, requiring more primary particles to get reasonable uncertainties, making the simulation more expensive in terms of CPU resources. In this sense, the 50-s overcooling transient problem becomes relatively easy to handle.

Comparing the pin-level results against the classic deterministic assembly-level solutions, we can conclude that the three implementations are consistent since global parameters are in excellent agreement. Higher peak values were obtained in the high-detail solution (*Max. Tdop*, *Max. Tclad*, *Max. voidf*) because of the different levels of detail in the models. For parameters like the DNB, where the assembly-based solutions could have considered some form factors (peak factors inside the assembly), the high-detail solution still predicts the minimum DNB value. The authors would like to highlight that DNB results for the three solutions could be biased since CAREM's nominal operation condition is out of range for using the Westinghouse-3 correlation. Nevertheless, the same differences in the results are expected for a more proper correlation. Due to the models' high-detail resolution and far fewer approximations, the Serpent/Subchanflow solution could be considered a reference solution for code-to-code comparisons, helping identify certain margins that classic approaches are not able to see because of their approximations, correct or improve safety factors, or assist in the design optimization.

Declaration of competing interest

The authors declare the following financial interests/personal relationships which may be considered as potential competing interests: Gianfranco Huaccho Zavala reports financial support was provided by Euratom Research and Training Programme. If there are other authors, they declare that they have no known competing financial interests or personal relationships that could have appeared to influence the work reported in this paper.

Acknowledgments

This work has received funding from the Euratom research and training program 2019–2020 under the grant agreement No 945063 H2020 McSAFER project. This work was performed on the Horeka supercomputer funded by the Ministry of Science, Research and the Arts Baden-Württemberg, Germany and by the Federal Ministry of Education and Research, Germany. The authors give special thanks to the colleagues from CNEA involved in the McSAFER project for defining the transient scenario and providing all the necessary data to perform this work.

Appendix. Kinetic constants

See Table A.8.

Data availability

The data that has been used is confidential.

Table A.8
8-group kinetic constants obtained with Serpent/Subchanflow for the converged steady-state using JEFF-3.1.1 NDL. 1σ is considered for the statistical uncertainty. A value without uncertainty means that its uncertainty is very small compared to the number obtained with the last significant digit.

β_{eff} [pcm]	733.9 ± 0.4
Λ [μs]	41.1
λ_i [1/s]	$\beta_i \times 10^5$
1.24667×10^{-2}	22.3 ± 0.1
2.82917×10^{-2}	106.6 ± 0.2
4.25244×10^{-2}	63.4 ± 0.1
1.33042×10^{-1}	139.6 ± 0.2
2.92467×10^{-1}	236.6 ± 0.3
6.66488×10^{-1}	77.0 ± 0.1
1.63478×10^{0}	64.8 ± 0.1
3.55460×10^{0}	23.6 ± 0.1

References

Almachi, J.C., Sánchez-Espinoza, V., Imke, U., 2021. Extension and validation of the SubChanFlow code for the thermo-hydraulic analysis of MTR cores with plate-type fuel assemblies. Nucl. Eng. Des. 379, 111221. http://dx.doi.org/10.1016/j.nucengdes.2021.111221.

Almachi, J.C., Sánchez-Espinoza, V., Imke, U., Stieglitz, R., Margulis, M., 2024. Validation of the dynamic simulation capabilities of Serpent2/Subchanflow using experimental data from the research reactor SPERT IV D-12/25. Nucl. Eng. Des. 418, 112840. http://dx.doi.org/10.1016/j.nucengdes.2023.112840.

Demazière, C., Sanchez-Espinoza, V.H., Chanaron, B., 2020. Advanced numerical simulation and modelling for reactor safety contributions from the CORTEX, HPMC, McSAFE and NURESAFE projects. EPJ Nucl. Sci. Technol. 6, 42. http://dx.doi.org/10.1051/epjn/2019006.

Ferraro, D., García, M., Imke, U., Valtavirta, V., Tuominem, R., Bilodid, Y., Leppänen, J., Sanchez-Espinoza, V., 2021a. Serpent/subchanflow coupled calculations for a VVER core at hot full power. PHYSOR2020 EPJ Web Conf. 247 (04006), http://dx.doi.org/10.1051/epjconf/202124704006.

Ferraro, D., García, M., Imke, U., Valtavirta, V., Tuominem, R., Leppänen, J., Sanchez-Espinoza, V., 2021b. Serpent/subchanflow coupled bunrup calculations for vver fuel assemblies. PHYSOR2020 EPJ Web Conf. 247 (04005), http://dx.doi.org/10.1051/epjconf/202124704005.

Ferraro, D., García, M., Valtavirta, V., Imke, U., Tuominen, R., Leppänen, J., Sanchez-Espinoza, V., 2020a. Serpent/SUBCHANFLOW pin-by-pin coupled transient calculations for a PWR minicore. Ann. Nucl. Energy 137, 107090. http://dx.doi.org/10.1016/j.anucene.2019.107090.

Ferraro, D., García, M., Valtavirta, V., Imke, U., Tuominen, R., Leppänen, J., Sanchez-Espinoza, V., 2020b. Serpent/SUBCHANFLOW pin-by-pin coupled transient calculations for the SPERT-IIIE hot full power tests. Ann. Nucl. Energy 142, 107387. http://dx.doi.org/10.1016/j.anucene.2020.107387.

Ferraro, D., Valtavirta, V., García, M., Imke, U., Tuominen, R., Leppänen, J., Sanchez-Espinoza, V., 2020c. OECD/NRC PWR MOX/UO2 core transient benchmark pin-by-pin solutions using Serpent/SUBCHANFLOW. Ann. Nucl. Energy 147, 107745. http://dx.doi.org/10.1016/j.anucene.2020.107745.

Fridman, E., Bilodid, Y., Dalinger, M., Lestani, H., Lopasso, E., Weir, A., Zalazar, R., Blanco, J.A., Mercatali, L., Sanchez E., V.H., Farda, A., Valtavirta, V., Jambrina, A., Seidl, M., De Meyer, D., Vocka, R., Frantisek, H., 2024. D3.4: State-of-the-art solutions for the transients scenarios in the four SMR cores and intercomparison between codes when applicable. http://dx.doi.org/10.5281/zenodo.10716851.

Garcia, M., Imke, U., Ferraro, D., Sanchez-Espinoza, V., Mercatali, L., 2019. Advanced modelling capabilities for pin-level subchannel analysis of PWR and VVER reactors. In: Vortrag gehalten auf 18th International Topical Meeting on Nuclear Reactor Thermal Hydraulics (NURETH 2019), Portland, OR, USA, 18.–23. August 2019.

Giménez, M.O., 2014. Technology development, desgin and safety features of CAREM-25. In: Interregional Workshop on Design, Technology, and Development Considerations for SMR, IAEA, Vienna, 2-5 of June.

Horeka, 2024. The horeka supercomputer at KIT (simon raffeiner, SCC/kit). https://www.nhr.kit.edu/userdocs/horeka/ (Accessed: 2024-07).

IAEA, 2014. Advances in Small Modular Reactor Technology Developments. A Supplement to: IAEA Advanced Reactors Information System (ARIS).

Imke, U., Sanchez, V.H., 2012. Validation of the subchannel code SUBCHANFLOW using the NUPEC PWR tests (PSBT). Sci. Technol. Nucl. Install. 2012, http://dx.doi.org/10.1155/2012/465059.

Leppänen, J., 2013a. Development of a dynamic simulation mode in serpent 2 monte carlo code. In: Proc. M&C 2013 Conf. Sun Valley, Idaho, May 5-9.

Leppänen, J., 2013b. Modeling of nonuniform density distributions in the serpent 2 Monte Carlo code. Nucl. Sci. Eng. 174 (3), 318–325. http://dx.doi.org/10.13182/NSE12-54.

Leppänen, J., Pusa, M., Viitanen, T., Valtavirta, V., Kaltiaisenaho, T., 2015. The Serpent Monte Carlo code: Status, development and applications in 2013. Ann. Nucl. Energy 82, 142–150. http://dx.doi.org/10.1016/j.anucene.2014.08.024.

Leppänen, J., Viitanen, T., Valtavirta, V., 2023. Multi-physics coupling scheme in the serpent 2 Monte Carlo code.

Magan, H.B., Delmastro, D.F., Markiewicz, M., Lopasso, E., Diez, F., Giménez, M., Rauschert, A., Halpert, S., Chocrón, M., Dezzutti, J.C., Pirani, H., Balbi, C., Fittipaldi, A., Schlamp, M., Murmis, G.M., Lis, H., 2011. CAREM project status. Sci. Technol. Nucl. Install. 2011, http://dx.doi.org/10.1155/2011/140373.

Marcel, C., Furci, H., Delmastro, D., Masson, V., 2013. Phenomenology involved in self-pressurized, natural circulation, low thermo-dynamic quality, nuclear reactors: The thermal–hydraulics of the CAREM-25 reactor. Nucl. Eng. Des. 254, 218–227. http://dx.doi.org/10.1016/j.nucengdes.2012.09.005.

Mercatali, L., Huaccho, G., Sanchez-Espinoza, V.-H., 2023a. Multiphysics modeling of a reactivity insertion transient at different fidelity levels in support to the safety assessment of a SMART-like small modular reactor. Front. Energy Res. 11, http://dx.doi.org/10.3389/fenrg.2023.1130554.

Mercatali, L., Lestani, H., Dalinger, M., Sanchez-Espinoza, V., 2023b. Modeling of an overcooling transient scenario in a CAREM-like small modular reactor. In: Proccedings of the 20th International Topical Meeting on Nuclear Reactor Thermal Hydraulics (NURETH-20), Washington, D.C..

OECD-NEA, 2024. The NEA small modular reactor. Dashboard: Second edition. Nucler Technol. Dev. Econ.

Sanchez-Espinoza, V.H., Gabriel, S., Suikkanen, H., Telkkä, J., Valtavirta, V., Bencik, M., Kliem, S., Queral, C., Farda, A., Abéguilé, F., Smith, P., Uffelen, P.V., Ammirabile, L., Seidl, M., Schneidesch, C., Grishchenko, D., Lestani, H., 2021a. The H2020 McSAFER project: Main goals, technical work program, and status. Energies 14 (19), http://dx.doi.org/10.3390/en14196348, URL https://www.mdpi.com/1996-1073/14/19/6348.

Sanchez-Espinoza, V.H., Mercatali, L., Leppänen, J., Hoogenboom, E., Vocka, R., Dufek, J., 2021b. The mcsafe project high-performance monte carlo based methods for safety demonstration: From proof of concept to industry applications. EPJ Web Conf. 247, 06004. http://dx.doi.org/10.1051/epjconf/202124706004.

Serpent Forum, 2024. Discussion forum for serpent users. https://ttuki.vtt.fi/serpent/ (Accessed: 2024-06).

Serpent Wiki, 2024. Serpent, a continuos-energy Monte Carlo neutron and photon transport code. https://serpent.vtt.fi/ (Accessed: 2024-06).

Stacey, W.M., 2006. Nuclear Reactor Physics, second ed. WILEY-VCH Verlag GmbH & Co. KGaA.

Valtavirta, V., Hessan, M., Leppänen, J., 2016. Delayed neutron emission model for time dependent simulations with the serpent 2 Monte Carlo code: First results. In: Proc. PHYSOR 2016 Conf. Sun Valley, United States.

Viitanen, T., Leppänen, J., 2014. Target motion sampling temperature treatment technique with elevated basis cross-section temperatures. Nucl. Sci. Eng. 177 (1), 77–89. http://dx.doi.org/10.13182/NSE13-37.